

Vorticity-Crystalline Order Coupling in Supersolids: Excitations and Re-entrant Phases

M. Schubert,^{1,*} K. Mukherjee,^{2,1} P. Stürmer,¹ and S. M. Reimann¹

¹*Mathematical Physics and NanoLund, LTH, Lund University, Box 118, 22100 Lund, Sweden*

²*Department of Engineering Science, University of Electro-Communications, Tokyo 182-8585, Japan*

(Dated: January 13, 2026)

Rotation is a natural tool in ultracold gases to break time-reversal symmetry, yet its impact on the collective excitations of supersolids remains largely unexplored. We show theoretically that tuning the rotation frequency, rather than the interparticle interactions, can trigger the superfluid-to-supersolid transition in Bose-Einstein condensates (dBECs). Computing excitation spectra in the presence of vortices and persistent currents, we uncover a vortex-driven *de-softening* mechanism whereby quantized vorticity elevates the gapless Goldstone mode to a finite-energy roton, restoring superfluidity. This effect results in re-entrant supersolid phases as a function of rotation frequency, revealing a fundamental coupling between topological defects and crystalline order.

Breaking time-reversal symmetry (TRS) underlies diverse phenomena from cosmological matter-antimatter asymmetry [1, 2] to chiral superconductivity [3]. In condensed matter, magnetic fields break TRS and lift Kramers degeneracy [4], enabling the quantum Hall effect [5, 6] and access to nontrivial topological states [7, 8]. Additionally, the competition between TRS-breaking fields and internal interactions often drives complex phase topographies, such as re-entrant superconductivity [9] and fractional quantum Hall transitions [10]. Analogously, in ultracold Bose and Fermi gases, external rotation breaks TRS by acting as a synthetic magnetic field [11, 12]. This induces the well-known hallmarks of superfluidity such as quantized vortices [13, 14] and persistent currents [15, 16], offering a highly controllable platform for exploring TRS-broken effects [17, 18].

Externally applied rotating magnetic fields have made it possible to nucleate vortices in dBECs in the superfluid (SF) as well as the emergent supersolid (SS) phases [19, 20]. The SS phase [21–25], defined by the simultaneous breaking of global gauge and continuous translational symmetries, has now been realized in several ultracold platforms [26–28] including lanthanide atomic gases [29–32], light-mediated cavity systems [33], and spin-orbit-coupled Bose gases [34]. Microscopically, the transition occurs due to the softening of a finite-momentum roton mode [35–41], which signals the shift from a homogeneous SF to a density-modulated SS state.

While such softening could be induced by flow velocities exceeding the Landau critical limit in superfluid ⁴He [42], current dipolar experiments [29–31, 40, 41, 43–45] typically access the roton instability through the precise tuning of anisotropic interparticle interactions instead of hydrodynamic flow. The resulting SS state comes with a rich hierarchy of collective excitations [46–53], including Higgs and Goldstone modes associated with spontaneous symmetry breaking [40, 47]. While these modes can reveal key system properties such as the order of the phase transition [54], they have so far been explored almost ex-

clusively within the manifold of time-reversal-invariant states.

In this Letter, we theoretically uncover spectral signatures of TRS breaking in rotating dBECs, revealing how the interplay between rotation and long-range interactions reconfigures a superfluid phase. Combining analytical insight with numerical calculations of excitation spectra in geometries hosting vortices and persistent currents, we show that rotation can induce supersolidity in otherwise SF regimes. Crucially, vortex nucleation in the ensuing SS state can effectively *de-soften* the Goldstone mode by lifting it back to a finite-energy roton excitation which restores the SF state. This novel mechanism yields a sequence of re-entrant supersolid pockets as a function of rotation frequency, where the discrete entry of vortices periodically suppresses and restores crystalline order. Our results open an experimentally feasible route to probe the impact of TRS breaking on dipolar supersolids, revealing a hitherto unknown fundamental coupling between quantized vorticity and density modulation.

Theoretical model— Let us consider a dilute, weakly interacting gas of ultracold dipolar atoms confined in a rotationally symmetric potential $V_{\text{trap}}(\mathbf{r})$ and subjected to an external rotation with angular velocity Ω . The short-range contact and long-range dipolar potential are modelled by $U_c = g \delta(\mathbf{r})$ with $g = \frac{4\pi\hbar^2 a_s}{M}$ and $U_{\text{dd}} = \frac{3\hbar^2 a_{\text{dd}}}{M} \frac{1-3\cos^2\Theta}{r^3}$, respectively. Here, M is the atomic mass, a_s is the tunable (via Feshbach resonance [55, 56]) s -wave scattering length, and a_{dd} denotes the dipolar length. Θ is the angle between \mathbf{r} and the polarization direction. To determine the ground states for a given Ω , we solve the extended Gross–Pitaevskii equation (eGPE) for the condensate wavefunction $\Psi(\mathbf{r}, t)$ in the rotating frame using imaginary-time propagation, including the Lee–Huang–Yang (LHY) beyond-mean-field correction in the local-density approximation [57–59], characterized by the coefficient g_{QF} (additional information is provided in Appendix A).

The excitation spectrum is obtained by linearizing the

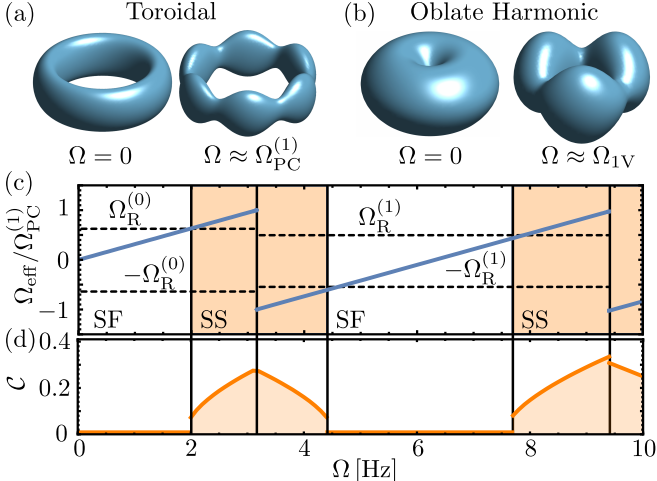


FIG. 1. **Rotation-induced supersolidity.** (a)-(b) Three-dimensional density isosurfaces (at 40% peak density) of the SF and SS states realized without and with external rotation Ω , respectively, at fixed scattering length a_s , in (a) a toroidal and (b) an oblate harmonic trap. The scattering lengths are $a_s = 92.8a_0$ in (a) and $87.4a_0$ in (b), with critical rotation frequencies $\Omega_{\text{PC}}^{(1)} \approx 3.2$ Hz and $\Omega_{1V} \approx 24.0$ Hz marking the nucleation of a single-quantized persistent current and a unit vortex, respectively. (c) The effective hydrodynamic flow velocity $\Omega_{\text{eff}} = \Omega - \Omega_{\text{GS}}$ (solid blue line) versus external rotation Ω for a toroidal trap of radius R , where $\Omega_{\text{GS}} = \hbar q/(MR^2)$ denotes the ground state angular velocity for a winding number q . The dashed black curve $\Omega_{\text{R}}^{(q)}$ denotes the critical angular velocity for roton softening (or Goldstone de-softening). The vertical black lines signify $\Omega_{\text{PC}}^{(q)}$, at which vortex nucleation reverses the effective flow, leading to a cyclic alternation between SF and SS phases as Ω varies. (d) Density contrast \mathcal{C} of the ground state showing the re-entrant supersolid pockets.

eGPE around the rotational ground state Ψ_0 , $\Psi(\mathbf{r}, t) = \Psi_0(\mathbf{r}) + \delta\Psi(\mathbf{r}, t)$, using the Bogoliubov ansatz $\delta\Psi(\mathbf{r}, t) = [u_j(\mathbf{r}) e^{-i\omega_j t} + v_j^*(\mathbf{r}) e^{i\omega_j t}] e^{-i\mu t/\hbar}$, where μ is the chemical potential in the rotating frame. The linearization leads to the Bogoliubov-de Gennes (BdG) equations,

$$\begin{pmatrix} \hat{\mathcal{L}} & \hat{\mathcal{D}} \\ -\hat{\mathcal{D}}^* & -\hat{\mathcal{L}}^* \end{pmatrix} \begin{pmatrix} u \\ v \end{pmatrix} = \hbar\omega \begin{pmatrix} u \\ v \end{pmatrix}, \quad (1)$$

where $\hat{\mathcal{L}}u = [-\frac{\hbar^2}{2m}\nabla^2 + V_{\text{trap}}(\mathbf{r}) + 2g|\Psi_0|^2 + U_{\text{dd}} * |\Psi_0|^2 + \frac{5}{2}g_{\text{QF}}|\Psi_0|^3 - \mu - \Omega\hat{L}_z]u + \Psi_0 U_{\text{dd}} * (\Psi_0^* u)$ and $\hat{\mathcal{D}}u = [g\Psi_0^2 + \frac{3}{2}g_{\text{QF}}|\Psi_0|\Psi_0^2]u + \Psi_0 U_{\text{dd}} * (\Psi_0 u)$. Solving these equations yields the excitation frequencies ω_j , the corresponding eigenfunctions u_j and v_j , as well as the density fluctuations of the ground state $\delta n_j = 2\text{Re}[(\Psi_0^* u_j + \Psi_0 v_j)e^{i\omega_j t}]$.

In the following, we consider parameters relevant to bosonic ^{162}Dy atoms ($a_{\text{dd}} = 130a_0$, with a_0 being the Bohr radius) and focus on angular excitation modes. In our azimuthally symmetric geometry, where $[\hat{\mathcal{L}}, \hat{L}_z] = [\hat{\mathcal{D}}, \hat{L}_z] = 0$, the modes of a SF are characterized by well-defined angular-momentum quantum numbers m , corresponding to eigenstates of \hat{L}_z , and dominate the low-energy spectrum. These excitations underpin the emergence

of supersolidity, which we quantify via the density contrast $\mathcal{C} = (n_{\text{max}} - n_{\text{min}})/(n_{\text{max}} + n_{\text{min}})$, where n_{max} and n_{min} are the local maximum and minimum densities [26, 60]. In the uniform SF regime $\mathcal{C} \rightarrow 0$, while $\mathcal{C} \rightarrow 1$ indicates a fully modulated state.

Flow-induced asymmetry in the excitations— To gain analytical insight into the angular excitations under rotation, we consider a toroidal geometry of radius R under tight confinement ($R \gg \sqrt{\hbar/M\omega_r}$). In this limit, the critical angular velocity for nucleating a persistent current in a SF with winding number q is $\Omega_{\text{PC}}^{(q)} = \hbar(q - \frac{1}{2})/(MR^2)$, independent of the interactions. Once such a current is established, the condensate acquires a finite circulation characterized by the ground state angular velocity $\Omega_{\text{GS}} = \hbar q/(MR^2)$. The resulting dynamics are governed by the effective hydrodynamic flow, defined by the relative angular velocity $\Omega_{\text{eff}} = \Omega - \Omega_{\text{GS}}$. The corresponding excitation spectrum can be obtained by solving Eq. (1) around the ground state $\Psi_0 \sim e^{iq\phi}$. Because the mode momentum m couples to the persistent current, it is useful to introduce the quantum number $\mathcal{M} = m - q$, which is also the angular momentum of the density fluctuations δn . Then, the excitation spectrum separates into two contributions and can be written as

$$\omega_{\mathcal{M}}^{(q)}(\Omega) = \tilde{\omega}_{\mathcal{M}}^{(q)} - \mathcal{M}\Omega_{\text{eff}}. \quad (2)$$

The first term in Eq. (2) incorporates interaction effects, including the long-range dipolar force and LHY corrections, and is independent of Ω . As a result, it preserves momentum-reversal symmetry ($\mathcal{M} \rightarrow -\mathcal{M}$). Meanwhile, the second term introduces a Galilean shift that removes the energy degeneracy between counter-propagating modes. As a result, the spectral splitting is determined entirely by the effective flow: $\omega_{-\mathcal{M}}^{(q)}(\Omega) - \omega_{\mathcal{M}}^{(q)}(\Omega) = 2\mathcal{M}\Omega_{\text{eff}}$. This provides a direct spectral signature of the persistent current. For $\Omega < \Omega_{\text{PC}}^{(1)}$, the ground state carries no circulation ($q = \Omega_{\text{GS}} = 0$), and the splitting follows the external rotation Ω . When $\Omega > \Omega_{\text{PC}}^{(1)}$, the system transitions into the $q = 1$ persistent-current state, causing the sign of the effective flow Ω_{eff} to reverse (see the thick blue line in Fig. 1(c), which shows Ω_{eff} as a function of Ω). This leads to mode swapping: the excitation mode that was previously lower in energy becomes the higher-energy one, and vice versa (see the subsequent discussion and Fig. 5 in Appendix B). As we will show, this exchange in energy ordering has a decisive impact on the crystalline order of the rotation-induced SS state.

Roton instability and re-entrant SS state— Equation (2) provides a direct criterion for identifying the dynamical instabilities of the system. We focus on the regime where the long-range dipolar interaction induces a pronounced momentum dependence, driving a rotational instability via roton modes labeled by $m = m_{\text{R}}$. In accordance with Eq. (2), the roton branches split: modes

with m_R having the same sign as Ω are lowered in energy (roton $^+$), while those with the opposite sign are pushed to higher energies (roton $^-$). As Ω increases, the energy of the roton $^+$ softens until it vanishes at $\omega_{m_R}^{(0)}(\Omega_R^{(0)}) = 0$, defining the critical angular velocity $\Omega_R^{(0)}$ for the roton instability in the absence of persistent current. For $\Omega > \Omega_R^{(0)}$, the system enters a SS phase characterized by spontaneous density modulation. In this phase, the roton $^+$ mode becomes a gapless Goldstone mode, while the roton $^-$ mode evolves into a gapped Higgs $^-$ mode.

Entering the persistent current state at $\Omega > \Omega_{PC}^{(1)}$ triggers the mode swapping. The previously counter-propagating Higgs $^-$ mode now becomes a Higgs $^+$ mode that progressively softens with increasing Ω . Once the effective velocity satisfies $\Omega_{eff} > -\Omega_R^{(1)}$, this excitation converts into a roton $^+$ mode. Simultaneously, the zero-energy Goldstone mode evolves into a gapped roton $^-$ mode. The de-softening of the Goldstone mode into a finite-energy roton drives the transition from the modulated SS state back into a SF one. As Ω increases toward the $q = 2$ threshold $\Omega_{PC}^{(2)}$, the enhanced relative flow again triggers a roton softening and a recovery of the SS density modulation. Consequently, the sequential nucleation of persistent current states drives a cyclic phase evolution, which manifests as discrete pockets of supersolidity, see Fig. 1(c)-(d), characterizing the re-entrant SS state.

Numerical results for toroidal traps— We now support our analytical insights by numerically solving the eGPE and BdG equations, Eq. (1). First, we consider a toroidal trapping potential, $V_{trap}(\mathbf{r}) = M\omega_r^2(\sqrt{x^2 + y^2 - R)^2/2} + M\omega_z^2z^2/2$, with trap frequencies $(\omega_r, \omega_z)/2\pi = (100, 120)$ Hz, radius $R = 2.8\mu\text{m}$, and atom number $N = 32400$. Dipolar BECs and their SS phases in toroidal geometries have so far only been studied theoretically [54, 61–68]; however, experimental realization is expected to follow soon. In the absence of rotation, our system undergoes a SF-SS transition at $a_s \approx 92.73a_0$, defining the quantum-critical point. Slightly above this threshold, we show the excitation spectra as a function of Ω at $a_s = 92.8a_0$ in Fig. 2(a).

At $\Omega = 0$, the spectrum exhibits a set of roton modes, along with higher-lying superfluid sound modes; see, for example, the profile ($f = u + v^*$) of the $m_R = 6$ roton mode in Fig. 2(a). Finite rotation lifts the degeneracy, causing the $m_R = 6$ roton $^+$ (roton $^-$) branch to soften (harden). At $\Omega_R^{(0)} \approx 2\pi \times 1.95$ Hz, the energy of the roton $^+$ mode vanishes, signaling the spontaneous breaking of azimuthal symmetry and the formation of a SS with $n_d = 6$ localized density sites; see also Fig. 1(a). Here, the roton $^+$ mode evolves into a gapless Goldstone mode, while the roton $^-$ becomes a gapped Higgs $^-$ mode.

A key highlight of our work is the nature of the phase transition. As illustrated in Fig. 2(b), the presence of a finite Higgs-mode gap at the critical point suggests a first-order character, which we explain within a Ginzburg-

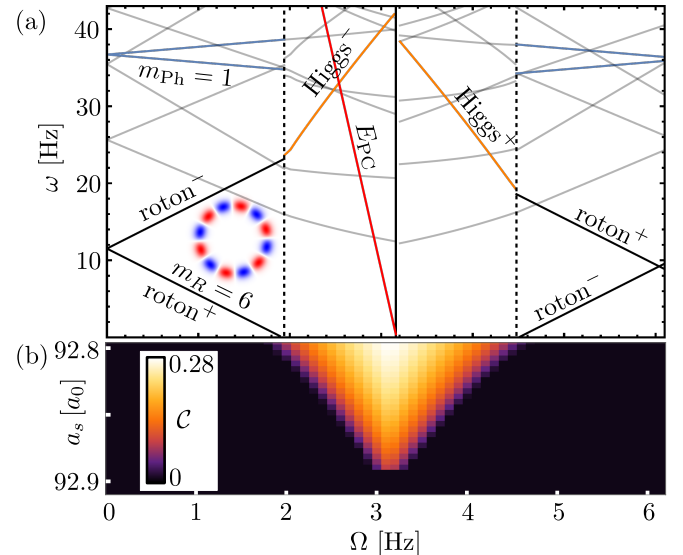


FIG. 2. **Excitation spectrum and phase diagram in toroidal geometry.** (a) BdG excitation energies vs. rotational velocity Ω at $a_s = 92.8a_0$. Black, blue, and orange lines denote the lowest roton ($m_R = 6$), superfluid phonon ($m_{Ph} = 1$), and Higgs modes, respectively. Vertical lines indicate the sequence of SF \rightarrow SS, vortex nucleation, and SS \rightarrow SF transitions. Signs \pm indicate angular momentum orientation relative to Ω . The red curve shows the persistent-current energy E_{PC} . (Inset) Bogoliubov mode profile f for the $m_R = 6$ roton at $\Omega = 0$ in the xy -plane (red/blue indicates negative/positive amplitude). (b) Density contrast C in the (Ω, a_s) plane, delineating the SF and SS regimes. See text for other parameters.

Landau framework [69, 70]. We express the energy in the rotating frame as $E' = E - L_z\Omega$. Taking the superfluid fraction f_s as the order parameter and treating the angular momentum classically, we approximate $L_z \approx I\Omega(1 - f_s)$, where I is the moment of inertia. This substitution introduces a term linear in f_s into the energy functional. Consequently, minimizing $E'(f_s)$ leads to a discontinuous jump in f_s at the transition. Crucially, while interaction-driven supersolid transitions in rings are typically second-order [54], the rotational breaking of TRS fundamentally shifts the transition to first-order.

The red line in Fig. 2 shows the energy difference $E_{PC} = E'(q = 1) - E'(q = 0)$, obtained from the eGPE, indicating that for $\Omega > \Omega_{PC}^{(1)} \approx 2\pi \times 3.2$ Hz the state with $q = 1$ becomes energetically favorable. Correspondingly, we observe the swapping of angular momenta of modes predicted by Eq. (2) and the subsequent reduction of the energy of the Higgs $^+$ mode. At $\Omega_R^{(1)} \approx 2\pi \times 4.47$ Hz, the system re-enters the SF phase, evidenced by the de-softening of the Goldstone mode. As Ω increases, this cycle repeats, generating a sequence of SF \rightarrow SS \rightarrow SF transitions [Fig. 1(d)]. This periodic recurrence, a re-entrant supersolidity, constitutes the main result of this work. While re-entrance in ultracold gases has been mostly studied in optical lattices [71–76], the phe-

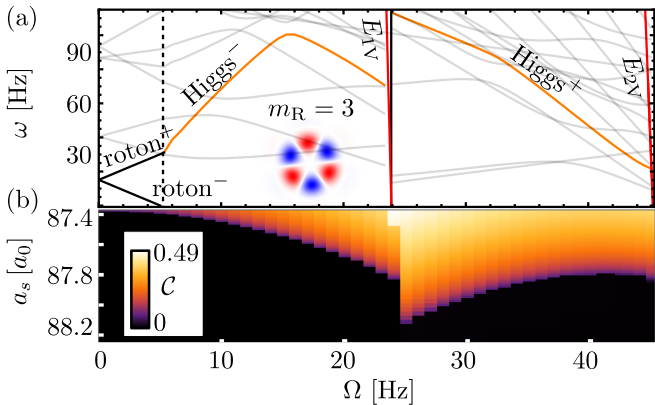


FIG. 3. Excitation spectrum and phase diagram in an oblate harmonic trap. (a) Excitation frequencies of rotons (black), Higgs (orange), and all other modes (gray) versus rotational angular velocity Ω . The dashed and solid vertical lines indicate $\Omega_R^{(0)}$ and Ω_{1V} , respectively, while the red lines denote the energy differences of the one- and two-vortex states relative to the ground state, E_{1V} and E_{2V} . Inset: mode profile f of the $m_R = 3$ roton driving the $\text{SF} \rightarrow \text{SS}$ transition. (b) Density-modulation contrast \mathcal{C} as a function of Ω and the s -wave scattering length a_s . Other parameters are given in the text.

nomenon reported here is fundamentally distinct; it is driven by the discrete nucleation of topological charge, which periodically restores and suppresses crystalline order. Since the critical velocities for roton softening and Goldstone de-softening depend on the winding number q , the rotation-induced SS phase is restricted to the intervals $|\Omega - \Omega_{GS}| < \Omega_R^{(q)}$. Notably, a phononic instability can also occur in the $m = m_{\text{ph}} = 1$ mode at a critical angular velocity $\Omega_{\text{Ph}} = \tilde{\omega}_1$. However, for a rotation-induced supersolid to emerge, the roton instability must occur first, requiring $\Omega_R^{(q)} < \Omega_{\text{Ph}}^{(q)}$. This condition is satisfied near the quantum-critical point, where the roton energies lie below phononic ones (see the blue curve in Fig. 2(a)).

In Fig. 2(b), we map the existence of the rotation-induced supersolid phase in the (Ω, a_s) parameter space using the density contrast \mathcal{C} . A finite \mathcal{C} , signaling SS formation, emerges over a broader range of Ω near the quantum critical point and a narrower range away from it. The maximum of \mathcal{C} occurs at $\Omega = \Omega_{\text{PC}}^{(1)} = 2\pi \times 3.2 \text{ Hz}$, in agreement with our analytical predictions. Since $\Omega_{\text{PC}}^{(1)}$ increases with decreasing ring radius R , this provides a route to stabilize the SS phase over a wider range of Ω .

Numerical results for oblate harmonic traps— To demonstrate that the rotationally induced SS phase is not restricted to specific geometries and to align our findings with established platforms [20, 78, 79], we next consider an oblate harmonic trap. We set $R = 0$ with trapping frequencies $(\omega_r, \omega_z) = 2\pi \times (125, 250) \text{ Hz}$ for a system containing $N = 2 \times 10^4$ atoms [50]. The resulting density isosurfaces for both non-rotating SF and rotating SS ground states are displayed in Fig. 1(b) above.

At $\Omega = 0$, the SF exhibits a density minimum at the trap center while preserving azimuthal symmetry. This configuration supports angular roton modes as the lowest-energy excitations, analogous to the toroidal geometry. Under rotation, the degeneracy of these modes is lifted, causing the branches to split and soften. Specifically, the $m_R = 3$ roton drives the transition to a SS state characterized by three distinct density maxima. This transition is marked by the emergence of zero-energy Goldstone and Higgs modes, as illustrated in Fig. 3(a). Note that we only highlight the roton and Higgs modes in Fig. 3(a), while plotting the rest of the spectrum in gray.

Notably, the finite central density in the harmonic trap renders vortex nucleation energetically more expensive than in the toroidal case [20, 80, 81]. This shifts the critical rotation frequencies for vortex formation to higher values [see the red lines in Fig. 3(a)]. Consequently, the parameter space supporting the rotation-induced SS phase is significantly expanded, as shown in the phase diagram in Fig. 3(b). For scattering lengths $a_s \lesssim 87.8 a_0$, we find that $\Omega_R^{(1)} < \Omega_{1V}$, indicating that the roton instability occurs before the onset of vortex entry. In contrast, for $a_s \gtrsim 87.8 a_0$, this ordering is reversed ($\Omega_R^{(1)} > \Omega_{1V}$). In the narrow intermediate regime $87.8 a_0 \lesssim a_s \lesssim 88.1 a_0$, the roton mode exhibits a characteristic de-softening behavior. Although mode coupling makes the rotational excitation spectra more intricate than in the toroidal case, the essential features of rotation-induced softening of the roton and de-softening of the Goldstone mode remain robust, as evident in Fig. 3.

Dynamical emergence of SS under rotation— To establish the experimental feasibility of our results, we perform real-time simulations incorporating phenomenological damping γ and noise in the initial state. Starting

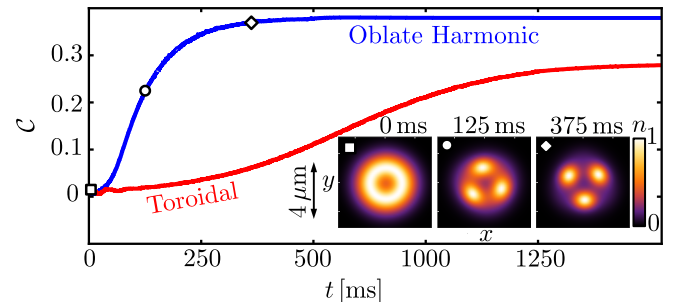


FIG. 4. Dynamical onset of supersolid order. Time evolution of the density contrast \mathcal{C} for toroidal (red) and oblate harmonic (blue) traps. Following a sudden quench of rotation to $\Omega/2\pi = 3 \text{ Hz}$ (toroidal) and 23 Hz (oblate harmonic), the nonrotating SF ground state undergoes spontaneous density modulation. (Inset) Snapshots of the integrated density $n(x, y)$ in the oblate harmonic trap at specific time intervals (see markers), refer to Ref. [77] for video of the dynamics. Scattering lengths are $a_s = 92.8 a_0$ (toroidal) and $87.4 a_0$ (oblate harmonic).

from a non-rotating SF ground state, we suddenly quench the rotation at $t = 0$ to $\Omega/2\pi = 23$ Hz for the oblate harmonic trap. This value sits slightly below the critical frequency $\Omega_{\text{PC}}^{(1)}/2\pi = 24$ Hz and precludes vortex nucleation while inducing pronounced azimuthal symmetry breaking. Figure 4 illustrates the time evolution of the density contrast \mathcal{C} (blue line), which grows from zero and saturates at $\mathcal{C} \approx 0.38$, signaling the formation of a stable SS phase. The insets in Fig. 4 display snapshots of the integrated 2D density profiles, $n(x, y) = \int |\Psi|^2 dz$, at selected time intervals (indicated by markers), capturing the emergence of the crystalline structure. An analogous dynamical evolution occurs for the toroidal geometry (red line in Fig. 4), demonstrating the robustness of the rotationally induced SS across different trapping potentials.

Conclusions and Outlook— We have investigated the Bogoliubov excitation spectra of rotating dipolar condensates. In geometries supporting angular excitations, such as toroidal and oblate harmonic traps, the breaking of TRS lifts roton degeneracy and triggers a first-order SF-SS transition. We uncover a nontrivial interplay between crystalline order and topological excitations, namely, persistent currents and quantized vortices, which drives a periodic sequence of SF \leftrightarrow SS transitions. This behavior is mediated by the de-softening of the gapless Goldstone mode and the simultaneous suppression of density modulations, giving rise to re-entrant SS phases, a phenomenon widely encountered in diverse systems such as liquid crystals [82], spin glasses [83], quantum hall states [84] and superconductivity [85].

Our work not only reveals an alternative to interaction-driven mechanisms for supersolidity via the excitation spectrum, but also paves the way for future studies of re-entrant phases in dBECs. Notably, these could be observed in diverse platforms, including dipolar molecules [86] and exciton–polariton condensates [87], and other lanthanide elements [29, 88], provided that: (i) the Hamiltonian supports low-energy angular excitations; (ii) the spectrum is concave; and (iii) the roton softening threshold Ω_R is the system’s lowest critical velocity. Utilizing rotation as a control parameter, our work enables SS in regimes where relatively weak long-range interactions would otherwise suppress it. Immediate extensions of this work include exploring finite-temperature effects [89] and further illuminating the other excitations, such as sound modes [90], revealing novel Josephson oscillations [91, 92] and shear waves [93] within the SS.

Acknowledgments—We are grateful to Tilman Pfau and Ralf Klemt, and the Stuttgart dysprosium team, as well as Tiziano Arnone Cardinale, Deepak Gaur and Lila Chergui for insightful discussions. Financial support from the Knut and Alice Wallenberg Foundation (Grant No. KAW2023.0322) and the Swedish Research Council (Grant No. 2022-03654 VR) is acknowledged. K. M. acknowledges financial support through the JSPS Postdoctoral Fellowship (Fellowship No. P25029).

* malte.schubert@fysik.lu.se

- [1] A. D. Sakharov, Violation of cp invariance, c asymmetry, and baryon asymmetry of the universe, *Pisma Zh. Eksp. Teor. Fiz.* **5**, 32 (1967), [JETP Lett. 5, 24 (1967)].
- [2] J. H. Christenson, J. W. Cronin, V. L. Fitch, and R. Turlay, Evidence for the 2π decay of the k_2^0 meson, *Phys. Rev. Lett.* **13**, 138 (1964).
- [3] A. P. Mackenzie and Y. Maeno, The superconductivity of Sr_2RuO_4 and the physics of spin-triplet pairing, *Rev. Mod. Phys.* **75**, 657 (2003).
- [4] H. A. Kramers, La théorie du pouvoir rotatoire paramagnétique, *Proc. Acad. Sci. Amsterdam* **33**, 959 (1930).
- [5] K. von Klitzing, G. Dorda, and M. Pepper, New method for high-precision determination of the fine-structure constant based on quantized hall resistance, *Phys. Rev. Lett.* **45**, 494 (1980).
- [6] R. B. Laughlin, Quantized Hall conductivity in two dimensions, *Phys. Rev. B* **23**, 5632 (1981).
- [7] M. Z. Hasan and C. L. Kane, Colloquium: Topological insulators, *Rev. Mod. Phys.* **82**, 3045 (2010).
- [8] X.-L. Qi and S.-C. Zhang, Topological insulators and superconductors, *Rev. Mod. Phys.* **83**, 1057 (2011).
- [9] H. W. Meul, C. Rossel, M. Decroux, O. Fischer, G. Remenyi, and A. Briggs, Observation of magnetic-field-induced superconductivity, *Phys. Rev. Lett.* **53**, 497 (1984).
- [10] J. P. Eisenstein, K. B. Lewis, A. S. Yeh, K. W. West, and L. N. Pfeiffer, Insulating and fractional quantum Hall states in the first excited Landau level, *Phys. Rev. Lett.* **88**, 076801 (2002).
- [11] A. L. Fetter, Rotating trapped Bose-Einstein condensates, *Rev. Mod. Phys.* **81**, 647 (2009).
- [12] J. Dalibard, F. Gerbier, G. Juzeliūnas, and P. Öhberg, Colloquium: Artificial gauge potentials for neutral atoms, *Rev. Mod. Phys.* **83**, 1523 (2011).
- [13] F. Chevy, K. W. Madison, and J. Dalibard, Measurement of the angular momentum of a rotating bose-einstein condensate, *Phys. Rev. Lett.* **85**, 2223 (2000); J. R. Abo-Shaeer, C. Raman, J. M. Vogels, and W. Ketterle, Observation of vortex lattices in Bose-Einstein Condensates, *Science* **292**, 476 (2001); P. Engels, I. Coddington, P. C. Haljan, V. Schweikhard, and E. A. Cornell, Observation of long-lived vortex aggregates in rapidly rotating Bose-Einstein Condensates, *Phys. Rev. Lett.* **90**, 170405 (2003).
- [14] M. W. Zwierlein, J. R. Abo-Shaeer, C. H. Schunck, A. Schirotzek, and W. Ketterle, Vortices and superfluidity in a strongly interacting Fermi gas, *Nature* **435**, 1047 (2005).
- [15] A. Ramanathan, K. C. Wright, S. R. Muniz, M. Zelan, W. T. Hill, C. J. Lobb, K. Helmerson, W. D. Phillips, and G. K. Campbell, Superflow in a toroidal bose-einstein condensate: An atomic squid, *Phys. Rev. Lett.* **106**, 130401 (2011); S. Moulder, S. Beattie, R. P. Smith, N. Tammuz, and Z. Hadzibabic, Quantized supercurrents in annular Bose-Einstein condensates, *Phys. Rev. A* **86**, 013603 (2012).
- [16] G. Del Pace, K. Xhani, A. Muzi Falconi, M. Fedrizzi, N. Grani, D. Hernandez Rajkov, M. Inguscio, F. Scazza, W. J. Kwon, and G. Roati, Imprinting persistent currents in tunable fermionic rings, *Phys. Rev. X* **12**, 041037

(2022); Y. Cai, D. G. Allman, P. Sabharwal, and K. C. Wright, Persistent currents in rings of ultracold fermionic atoms, *Phys. Rev. Lett.* **128**, 150401 (2022).

[17] B. Mukherjee, A. Shaffer, P. B. Patel, Z. Yan, C. C. Wilson, V. Crépel, R. J. Fletcher, and M. Zwierlein, Crystallization of bosonic quantum Hall states in a rotating quantum gas, *Nature* **601**, 58 (2022).

[18] R. Yao, S. Chi, B. Mukherjee, A. Shaffer, M. Zwierlein, and R. J. Fletcher, Observation of chiral edge transport in a rapidly rotating quantum gas, *Nat. Phys.* **20**, 1726 (2024).

[19] L. Klaus, T. Bland, E. Poli, C. Politi, G. Lamporesi, E. Casotti, R. N. Bisset, M. J. Mark, and F. Ferlaino, Observation of vortices and vortex stripes in a dipolar condensate, *Nature Physics* **18**, 1453 (2022).

[20] E. Casotti, E. Poli, L. Klaus, A. Litvinov, C. Ulm, C. Politi, M. J. Mark, T. Bland, and F. Ferlaino, Observation of vortices in a dipolar supersolid, *Nature* **635**, 327 (2024).

[21] E. P. Gross, Unified theory of interacting bosons, *Phys. Rev.* **106**, 161 (1957).

[22] C. N. Yang, Concept of off-diagonal long-range order and the quantum phases of liquid he and of superconductors, *Rev. Mod. Phys.* **34**, 694 (1962).

[23] A. F. Andreev and I. M. Lifshitz, Quantum Theory of Defects In Crystals, *J. Exp. Theo. Phys.* **56**, 2057 (1969).

[24] G. V. Chester, Speculations on Bose-Einstein Condensation and Quantum Crystals, *Phys. Rev. A* **2**, 256 (1970).

[25] M. Boninsegni and N. V. Prokof'ev, Colloquium: Supersolids: What and where are they?, *Rev. Mod. Phys.* **84**, 759 (2012).

[26] L. Chomaz, I. Ferrier-Barbut, F. Ferlaino, B. Laburthe-Tolra, B. L. Lev, and T. Pfau, Dipolar physics: a review of experiments with magnetic quantum gases, *Reports on Progress in Physics* **86**, 026401 (2023).

[27] K. Mukherjee, T. A. Cardinale, L. Chergui, P. Stürmer, and S. Reimann, Droplets and supersolids in ultra-cold atomic quantum gases, *The European Physical Journal Special Topics* **232**, 3417 (2023).

[28] A. Recati and S. Stringari, Supersolidity in ultracold dipolar gases, *Nature Reviews Physics* **5**, 735 (2023).

[29] L. Chomaz, D. Petter, P. Ilzhöfer, G. Natale, A. Trautmann, C. Politi, G. Durastante, R. M. W. van Bijnen, A. Patscheider, M. Sohmen, M. J. Mark, and F. Ferlaino, Long-lived and transient supersolid behaviors in dipolar quantum gases, *Phys. Rev. X* **9**, 021012 (2019).

[30] F. Böttcher, J.-N. Schmidt, M. Wenzel, J. Hertkorn, M. Guo, T. Langen, and T. Pfau, Transient supersolid properties in an array of dipolar quantum droplets, *Phys. Rev. X* **9**, 011051 (2019).

[31] L. Tanzi, E. Lucioni, F. Famà, J. Catani, A. Fioretti, C. Gabbanini, R. N. Bisset, L. Santos, and G. Modugno, Observation of a Dipolar Quantum Gas with Metastable Supersolid Properties, *Phys. Rev. Lett.* **122**, 130405 (2019).

[32] M. A. Norcia, C. Politi, L. Klaus, E. Poli, M. Sohmen, M. J. Mark, R. N. Bisset, L. Santos, and F. Ferlaino, Two-dimensional supersolidity in a dipolar quantum gas, *Nature* **596**, 357 (2021).

[33] J. Leonard, A. Morales, P. Zupancic, T. Esslinger, and T. Donner, A stripe phase with supersolid properties in spin-orbit-coupled bose-einstein condensates, *Nature* **543**, 87 (2017).

[34] J.-R. Li, J. Lee, W. Huang, S. Burchesky, B. Shteynas, F. C. Top, A. O. Jamison, and W. Ketterle, A stripe phase with supersolid properties in spin-orbit-coupled bose-einstein condensates, *Nature* **543**, 91–94 (2017).

[35] Y. Pomeau and S. Rica, Dynamics of a model of supersolid, *Phys. Rev. Lett.* **72**, 2426 (1994).

[36] L. Santos, G. V. Shlyapnikov, and M. Lewenstein, Roton-Maxon Spectrum and Stability of Trapped Dipolar Bose-Einstein Condensates, *Phys. Rev. Lett.* **90**, 250403 (2003).

[37] R. M. Wilson, S. Ronen, J. L. Bohn, and H. Pu, Manifestations of the roton mode in dipolar Bose-Einstein condensates, *Phys. Rev. Lett.* **100**, 245302 (2008).

[38] P. B. Blakie, D. Baillie, and R. N. Bisset, Roton spectroscopy in a harmonically trapped dipolar Bose-Einstein condensate, *Phys. Rev. A* **86**, 021604 (2012).

[39] A. D. Martin and P. B. Blakie, Stability and structure of an anisotropically trapped dipolar bose-einstein condensate: Angular and linear rotons, *Phys. Rev. A* **86**, 053623 (2012).

[40] L. Chomaz, R. M. W. van Bijnen, D. Petter, G. Faraoni, S. Baier, J. H. Becher, M. J. Mark, F. Wächtler, L. Santos, and F. Ferlaino, Observation of roton mode population in a dipolar quantum gas, *Nat. Phys.* **14**, 442 (2018).

[41] J.-N. Schmidt, J. Hertkorn, M. Guo, F. Böttcher, M. Schmidt, K. S. H. Ng, S. D. Graham, T. Langen, M. Zwierlein, and T. Pfau, Roton excitations in an oblate dipolar quantum gas, *Phys. Rev. Lett.* **126**, 193002 (2021).

[42] L. Landau, Theory of the superfluidity of helium ii, *Phys. Rev.* **60**, 356 (1941); L. P. Pitaevskii, Layered structure of Bose crystals, *JETP Lett.* **39**, 511 (1984), [Pis'ma Zh. Eksp. Teor. Fiz. 39, 423 (1984)]; F. Ancilotto, F. Dalfovo, L. P. Pitaevskii, and F. Toigo, Density pattern in supercritical flow of liquid ^4He , *Phys. Rev. B* **71**, 104530 (2005).

[43] I. Ferrier-Barbut, H. Kadau, M. Schmitt, M. Wenzel, and T. Pfau, Observation of Quantum Droplets in a Strongly Dipolar Bose Gas, *Phys. Rev. Lett.* **116**, 215301 (2016).

[44] M. Schmitt, M. Wenzel, F. Böttcher, I. Ferrier-Barbut, and T. Pfau, Self-bound droplets of a dilute magnetic quantum liquid, *Nature* **539**, 259 (2016).

[45] L. Chomaz, S. Baier, D. Petter, M. J. Mark, F. Wächtler, L. Santos, and F. Ferlaino, Quantum-Fluctuation-Driven Crossover from a Dilute Bose-Einstein Condensate to a Macrodroplet in a Dipolar Quantum Fluid, *Phys. Rev. X* **6**, 041039 (2016).

[46] G. Natale, R. M. W. van Bijnen, A. Patscheider, D. Petter, M. J. Mark, L. Chomaz, and F. Ferlaino, Excitation spectrum of a trapped dipolar supersolid and its experimental evidence, *Phys. Rev. Lett.* **123**, 050402 (2019).

[47] D. Petter, G. Natale, R. M. W. van Bijnen, A. Patscheider, M. J. Mark, L. Chomaz, and F. Ferlaino, Probing the Roton Excitation Spectrum of a Stable Dipolar Bose Gas, *Phys. Rev. Lett.* **122**, 183401 (2019).

[48] M. Guo, F. Böttcher, J. Hertkorn, J.-N. Schmidt, M. Wenzel, H. P. Büchler, T. Langen, and T. Pfau, The low-energy Goldstone mode in a trapped dipolar supersolid, *Nature* **574**, 386 (2019).

[49] J. Hertkorn, F. Böttcher, M. Guo, J. N. Schmidt, T. Langen, H. P. Büchler, and T. Pfau, Fate of the amplitude mode in a trapped dipolar supersolid, *Phys. Rev. Lett.* **123**, 193002 (2019).

[50] J. Hertkorn, J.-N. Schmidt, M. Guo, F. Böttcher, K. S. H. Ng, S. D. Graham, P. Uerlings, H. P. Büchler, T. Lan-

gen, M. Zwierlein, and T. Pfau, Supersolidity in two-dimensional trapped dipolar droplet arrays, *Phys. Rev. Lett.* **127**, 155301 (2021).

[51] T. Ilg and H. P. Büchler, Ground-state stability and excitation spectrum of a one-dimensional dipolar supersolid, *Phys. Rev. A* **107**, 013314 (2023).

[52] W. Kirkby, A.-C. Lee, D. Baillie, T. Bland, F. Ferlaino, P. B. Blakie, and R. N. Bisset, Excitations of a binary dipolar supersolid, *Phys. Rev. Lett.* **133**, 103401 (2024).

[53] E. Poli, D. Baillie, F. Ferlaino, and P. B. Blakie, Excitations of a two-dimensional supersolid, *Phys. Rev. A* **110**, 053301 (2024).

[54] J. Hertkorn, P. Stürmer, K. Mukherjee, K. S. Ng, P. Uerlings, F. Hellstern, L. Lavoine, S. Reimann, T. Pfau, and R. Klemt, Decoupled sound and amplitude modes in trapped dipolar supersolids, *Physical Review Research* **6**, L042056 (2024).

[55] C. Chin, R. Grimm, P. Julienne, and E. Tiesinga, Feshbach resonances in ultracold gases, *Rev. Mod. Phys.* **82**, 1225 (2010).

[56] Y. Tang, A. Sykes, N. Q. Burdick, J. L. Bohn, and B. L. Lev, *s*-wave scattering lengths of the strongly dipolar bosons ^{162}Dy and ^{164}Dy , *Phys. Rev. A* **92**, 022703 (2015).

[57] A. R. P. Lima and A. Pelster, Quantum fluctuations in dipolar Bose gases, *Phys. Rev. A* **84**, 041604 (2011).

[58] A. R. P. Lima and A. Pelster, Beyond mean-field low-lying excitations of dipolar Bose gases, *Phys. Rev. A* **86**, 063609 (2012).

[59] F. Wächtler and L. Santos, Ground-state properties and elementary excitations of quantum droplets in dipolar Bose-Einstein condensates, *Phys. Rev. A* **94**, 043618 (2016).

[60] K. Mukherjee, T. A. Cardinale, and S. M. Reimann, Selective rotation and attractive persistent currents in antidipolar ring supersolids, *Phys. Rev. A* **111**, 033304 (2025).

[61] M. Abad, M. Guilleumas, R. Mayol, M. Pi, and D. M. Jezek, Dipolar condensates confined in a toroidal trap: Ground state and vortices, *Phys. Rev. A* **81**, 043619 (2010).

[62] M. Abad, M. Guilleumas, R. Mayol, M. Pi, and D. M. Jezek, Phase slippage and self-trapping in a self-induced bosonic Josephson junction, *Phys. Rev. A* **84**, 035601 (2011).

[63] M. N. Tengstrand, D. Boholm, R. Sachdeva, J. Bengtsson, and S. M. Reimann, Persistent currents in toroidal dipolar supersolids, *Phys. Rev. A* **103**, 013313 (2021).

[64] M. N. Tengstrand, and P. Stürmer, and J. Ribbing, and S. M. Reimann, Toroidal dipolar supersolid with a rotating weak link, *Phys. Rev. A* **107**, 063316 (2023).

[65] M. Šindik, T. Zawiślak, A. Recati, and S. Stringari, Sound, superfluidity, and layer compressibility in a ring dipolar supersolid, *Phys. Rev. Lett.* **132**, 146001 (2024).

[66] K. Mukherjee, M. Schubert, R. Klemt, T. Bland, T. Pfau, and S. M. Reimann, Quantum carpets of Higgs quasi-particles in a supersolid, *Phys. Rev. Lett.* **135**, 223402 (2025).

[67] M. Schubert, K. Mukherjee, T. Pfau, and S. M. Reimann, Josephson vortices and persistent current in a double-ring supersolid system, *Phys. Rev. Res.* **7**, 033110 (2025).

[68] N. Preti, N. Antolini, C. Drevon, P. Lombardi, A. Fioretti, C. Gabbanini, G. Ferioli, G. Modugno, and G. Biagioni, Single-fluid model for rotating an- nular supersolids and its experimental implications, *arXiv:2510.26753* (2025).

[69] Y.-C. Zhang, F. Maucher, and T. Pohl, Supersolidity around a critical point in dipolar Bose Einstein condensates, *Phys. Rev. Lett.* **123**, 15301 (2019).

[70] G. Biagioni, N. Antolini, A. Alaña, M. Modugno, A. Fioretti, C. Gabbanini, L. Tanzi, and G. Modugno, Dimensional crossover in the superfluid-supersolid quantum phase transition, *Phys. Rev. X* **12**, 021019 (2022).

[71] H. Kleinert, S. Schmidt, and A. Pelster, Reentrant phenomenon in the quantum phase transitions of a gas of bosons trapped in an optical lattice, *Phys. Rev. Lett.* **93**, 160402 (2004).

[72] Z. Shen, L. Radzihovsky, and V. Gurarie, Reentrant bcs-bec crossover and a superfluid-insulator transition in optical lattices, *Phys. Rev. Lett.* **109**, 245302 (2012).

[73] L. Radzihovsky, Reentrant supersolidity, *arXiv:2311.04266* (2023).

[74] A. M. Piekarska and T. K. Kopeć, Reentrant phase transitions involving glassy and superfluid orders in the random hopping bose-hubbard model, *Physica A: Statistical Mechanics and its Applications* **609**, 128360 (2023).

[75] A. Krzywicka and T. P. Polak, Reentrant phase behavior in systems with density-induced tunneling, *Sci. Rep.* **14**, 10364 (2024).

[76] S.-H. Ding, L.-J. Lang, Q. Zhu, and L. He, Interaction-induced reentrance of bose glass and quench dynamics of bose gases in twisted bilayer and quasicrystal optical lattices, *Phys. Rev. A* **112**, 033322 (2025).

[77] See supplementary material for a video of the full dynamics, which show the density isosurfaces in the rotating frame for the oblate harmonic trap taken at 20% and 40% of the maximum density.

[78] Schmidt, J.-N. and Hertkorn, J. and Guo, M. and Böttcher, F. and Schmidt, M. and Ng, K. S. H. and Graham, S. D. and Langen, T. and Zwierlein, M. and Pfau, T., Roton Excitations in an Oblate Dipolar Quantum Gas, *Phys. Rev. Lett.* **126**, 193002 (2021).

[79] P. Molignini, Beyond-mean-field phases of rotating dipolar condensates in the strongly correlated regime, *Journal of Physics: Condensed Matter* **37**, 445401 (2025).

[80] S. M. Roccuzzo, A. Gallemí, A. Recati, and S. Stringari, Rotating a Supersolid Dipolar Gas, *Phys. Rev. Lett.* **124**, 045702 (2020).

[81] M. Šindik, A. Recati, S. M. Roccuzzo, L. Santos, and S. Stringari, Creation and robustness of quantized vortices in a dipolar supersolid when crossing the superfluid-to-supersolid transition, *Phys. Rev. A* **106**, L061303 (2022).

[82] P. E. Cladis, New liquid-crystal phase diagram: An isotropic-nematic-smectic-*a*-nematic transitions, *Phys. Rev. Lett.* **35**, 48 (1975).

[83] M. Gabay and G. Toulouse, Coexistence of spin-glass and ferromagnetic orderings, *Phys. Rev. Lett.* **47**, 201 (1981); G. Aeppli, S. M. Shapiro, R. J. Birgeneau, and H. S. Chen, Spin-wave dynamics in a reentrant spin-glass, *Phys. Rev. B* **25**, 4882 (1982).

[84] K. B. Cooper, M. P. Lilly, J. P. Eisenstein, L. N. Pfeiffer, and K. W. West, Insulating phases of two-dimensional electrons in high landau levels: Observation of sharp thresholds to conduction, *Phys. Rev. B* **60**, R11285 (1999).

[85] V. Jaccarino and M. Peter, Ultra-high-field superconductivity, *Phys. Rev. Lett.* **9**, 290 (1962).

[86] S. Zhang, W. Yuan, N. Bigagli, H. Kwak, T. Karman,

I. Stevenson, and S. Will, Observation of self-bound droplets of ultracold dipolar molecules, [arXiv preprint arXiv:2507.15208 \(2025\)](#); W. Zhang, H. Liu, F. Deng, K. Chen, S. Yi, and T. Shi, Supersolid phases in ultracold gases of microwave shielded polar molecules, [arXiv preprint arXiv:2506.23820 \(2025\)](#).

[87] F. Manni, K. G. Lagoudakis, T. C. H. Liew, R. André, and B. Deveaud-Plédran, Spontaneous pattern formation in a polariton condensate, [Phys. Rev. Lett. 107, 106401 \(2011\)](#); D. Trypogeorgos, A. Gianfrate, M. Landini, D. Nigro, D. Gerace, I. Carusotto, F. Riminiucci, K. W. Baldwin, L. N. Pfeiffer, G. I. Martone, M. De Giorgi, D. Ballarini, and D. Sanvitto, Emerging supersolidity in photonic-crystal polariton condensates, [Nature 639, 337 \(2025\)](#).

[88] Y. Miyazawa, R. Inoue, H. Matsui, G. Nomura, and M. Kozuma, Bose-einstein condensation of europium, [Phys. Rev. Lett. 129, 223401 \(2022\)](#).

[89] J. Sánchez-Baena, C. Politi, F. Maucher, F. Ferlaino, and T. Pohl, Heating a dipolar quantum fluid into a solid, [Nature Communications 14, 1868 \(2023\)](#).

[90] T. Zawiślak, M. Sindik, S. Stringari, and A. Recati, Anomalous doppler effect in superfluid and supersolid atomic gases, [Phys. Rev. Lett. 134, 226001 \(2025\)](#).

[91] G. Biagioni, N. Antolini, B. Donelli, L. Pezzè, A. Smerzi, M. Fattori, A. Fioretti, C. Gabbanini, M. Inguscio, L. Tanzi, *et al.*, Measurement of the superfluid fraction of a supersolid by josephson effect, [Nature 629, 773 \(2024\)](#).

[92] L. Platt, D. Baillie, and P. Blakie, Sound waves and fluctuations in one-dimensional supersolids, [Physical Review A 110, 023320 \(2024\)](#).

[93] P. Senarath Yapa and T. Bland, Anomalous dispersion of shear waves in dipolar supersolids, [Phys. Rev. A 112, L021303 \(2025\)](#).

[94] R. N. Bisset, R. M. Wilson, D. Baillie, and P. B. Blakie, Ground-state phase diagram of a dipolar condensate with quantum fluctuations, [Phys. Rev. A 94, 033619 \(2016\)](#).

END MATTER

Appendix A— In this section, we describe the numerical methods employed to obtain the ground states and dynamical properties presented in the main text. All simulations are performed at zero temperature within the mean-field framework of the eGPE [43, 45, 59, 94]. The time evolution of the condensate wavefunction $\Psi(\mathbf{r}, t)$ in the rotating frame is governed by:

$$i\hbar \frac{\partial \Psi(\mathbf{r}, t)}{\partial t} = (\hat{\mathcal{H}} - \Omega \hat{L}_z) \Psi(\mathbf{r}, t), \quad (3)$$

where the eGPE operator $\hat{\mathcal{H}}$ is defined as:

$$\begin{aligned} \hat{\mathcal{H}} = & -\frac{\hbar^2}{2M} \nabla^2 + V_{\text{trap}}(\mathbf{r}) + g|\Psi|^2 + g_{\text{QF}}|\Psi|^3 \\ & + \int d^3\mathbf{r}' U_{\text{dd}}(\mathbf{r} - \mathbf{r}') |\Psi(\mathbf{r}', t)|^2. \end{aligned} \quad (4)$$

The external potential $V_{\text{trap}}(\mathbf{r})$ accounts for the static confinement, which in this work is either a toroidal or

an oblate harmonic potential. Quantum fluctuations are incorporated via the LHY correction with the coefficient $g_{\text{QF}} = \frac{32}{3}g\sqrt{a_s^3/\pi}(1 + \frac{3}{2}\epsilon_{\text{dd}}^2)$, where $\epsilon_{\text{dd}} = a_{\text{dd}}/a_s$.

The corresponding energy functional associated with the eGPE, the minimization of which yields the stationary states, is given by $E'[\Psi] = E[\Psi] - \Omega L_z$ with

$$\begin{aligned} E[\Psi] = & \int d^3\mathbf{r} \left[\frac{\hbar^2}{2M} |\nabla \Psi|^2 + V_{\text{trap}}(\mathbf{r}) |\Psi|^2 + \frac{g}{2} |\Psi|^4 \right. \\ & \left. + \frac{2}{5} g_{\text{QF}} |\Psi|^5 \right] + \frac{1}{2} \iint d^3\mathbf{r} d^3\mathbf{r}' \\ & \times |\Psi(\mathbf{r})|^2 U_{\text{dd}}(\mathbf{r} - \mathbf{r}') |\Psi(\mathbf{r}')|^2. \end{aligned} \quad (5)$$

For numerical implementation, the eGPE is rescaled into a dimensionless form using a characteristic length scale $l_s = 10^{-6} \text{ m}$ and time scale $t_s = Ml_s^2/\hbar$. Ground states are obtained via imaginary-time propagation using a split-step Fourier spectral method. To analyze the dynamical response and excitation spectra, we perform subsequent real-time propagation with a time step of $\Delta t = 10^{-4} t_s$. The nonlocal dipolar term is evaluated efficiently as a convolution in momentum space, utilizing a spherical cutoff for the interaction kernel to eliminate aliasing effects and spurious interactions between periodic images.

Simulations are conducted in a three-dimensional box with dimensions $L_x = L_y = L_z = 22 \mu\text{m}$. We confirmed numerical convergence by comparing results across grid resolutions of $128 \times 128 \times 64$ and $256 \times 256 \times 64$, noting that the accuracy of the BdG excitation frequencies depends primarily on the physical box size.

To model the dynamics of the rotation-induced supersolid state, we include a phenomenological damping term in the eGPE:

$$(i - \gamma)\hbar \frac{\partial \Psi}{\partial t} = (\hat{\mathcal{H}} - \Omega \hat{L}_z) \Psi, \quad (6)$$

where $\gamma \ll 1$ is a small dimensionless damping parameter. This term accounts for dissipative processes and facilitates the system's relaxation toward stable dynamical configurations. For the real-time dynamics discussed in the main text, we have used $\gamma = 0.035$ for the toroidal trap and $\gamma = 0.02$ for the oblate harmonic trap. At $t = 0$, we also introduce a small perturbation to account for experimental inhomogeneities and to break the angular symmetry.

Appendix B— To gain analytical insight into the excitation spectrum under rotation, we consider a superfluid confined to a narrow ring of radius R satisfying $R \gg \sqrt{\hbar/M\omega_r}$. We derive the excitation energies as a function of the external rotation Ω and the ground-state winding number q by assuming the solutions for the non-rotating case ($\Omega = q = 0$) are known. This reference set of solutions is denoted by:

$$(\tilde{\omega}_m, \tilde{u}_m e^{im\phi}, \tilde{v}_m e^{im\phi}), \quad (7)$$

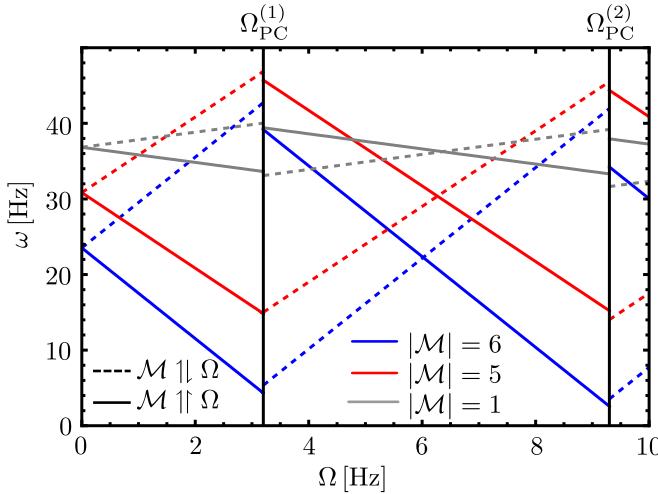


FIG. 5. **Mode-Swapping in a rotating toroidal Superfluid.** The energies of the six lowest excitations ($\mathcal{M} = \pm 6, \pm 5, \pm 1$) for the system from Fig. 2 in the main text with $a_s = 93a_0$. The modes propagating in the direction of Ω are shown as solid lines, whereas we indicate modes propagating antiparallel to Ω as dashed lines. The vertical black lines indicate the critical rotation frequencies at which persistent currents are generated, corresponding to mode swapping.

where \tilde{u}_m and \tilde{v}_m represent the quasiparticle amplitudes in the transversal (r, z) directions.

We now demonstrate that the vector

$$\begin{pmatrix} u \\ v \end{pmatrix} = \begin{pmatrix} \tilde{u}_M e^{im\phi} \\ \tilde{v}_M e^{i(m-2q)\phi} \end{pmatrix} \quad (8)$$

is a valid solution to the BdG equations and leads to the dispersion relation utilized in the main text. We begin by employing the tight-confinement approximation for the gradient operator, $\nabla_\phi \approx \frac{1}{R} \frac{\partial}{\partial \phi}$. Furthermore, we approximate the ground-state wavefunction as:

$$\Psi(\mathbf{r}) \approx |\tilde{\Psi}(r, z)| e^{iq\phi}, \quad (9)$$

assuming that the radial density profile is approximately independent of the circulation q . Under these conditions,

the chemical potential can be expressed as:

$$\mu = \tilde{\mu} + \frac{q^2 \hbar^2}{2MR^2} - \Omega \hbar q, \quad (10)$$

where $\tilde{\mu}$ is the chemical potential for the non-rotating system ($\Omega = q = 0$).

Inserting these expressions into the BdG equations and performing straightforward algebraic manipulation yields the following expression for the dispersion relation $\omega_{\mathcal{M}}^{(q)}$:

$$\omega_{\mathcal{M}}^{(q)}(\Omega) = \tilde{\omega}_{\mathcal{M}} + \frac{mq\hbar}{MR^2} - \frac{q^2\hbar}{MR^2} + \Omega(q - m). \quad (11)$$

By introducing the fluctuation momentum $\mathcal{M} = m - q$, we recover the Galilean-shifted dispersion relation:

$$\omega_{\mathcal{M}}^{(q)}(\Omega) = \tilde{\omega}_{\mathcal{M}} - \mathcal{M} \left(\Omega - \frac{q\hbar}{MR^2} \right) = \tilde{\omega}_{\mathcal{M}} - \mathcal{M} \Omega_{\text{eff}}. \quad (12)$$

It is important to note that the derivation above strictly holds when the radial and angular motions are decoupled ($R \gg \sqrt{\hbar/M\omega_r}$). In our numerical simulations, this condition is not perfectly satisfied, and the particle density $|\Psi|^2$ acquires a slight q -dependence due to radial centrifugal shifts, see Fig. 5. Due to the radial coupling, the energies are not continuous, $\omega_{\mathcal{M}}^{(q-1)}(\Omega_{\text{PC}}^{(q)}) \neq \omega_{-\mathcal{M}}^q(\Omega_{\text{PC}}^{(q)})$. However, we find that the general form of the dispersion remains robust if one replaces the intrinsic frequency with a q -dependent one, $\tilde{\omega}_{\mathcal{M}} \rightarrow \tilde{\omega}_{\mathcal{M}}^{(q)}$. This replacement allows us to construct the full spectrum by combining the numerically calculated excitation energies at different q values with the analytical Doppler shift, rather than solving the full BdG problem for every value of Ω .

This method remains valid as long as the radial trapping frequency dominates the rotation ($\omega_r \gg \Omega$). If this condition is violated, centrifugal effects would cause the density to depend explicitly on Ω . Our numerical analysis confirms that such effects are negligible for the parameter regimes studied in the main text. Nevertheless, all results presented in the main text are cross-verified by solving the full, non-decoupled BdG problem to ensure that all rotational and interaction effects are rigorously captured.